Biosensors and Bioelectronics 213 (2022) 114433

Contents lists available at ScienceDirect

Biosensors and Bioelectronics

journal homepage: www.elsevier.com/locate/bios

2D transparent few-layered hydrogen substituted graphdiyne nano-interface for unprecedented ultralow ANXA2 cancer biomarker detection

Dipti Chauhan [a], Yogesh Kumar [a], Ramesh Chandra [b,*], Suveen Kumar [a,*]

[a] Department of Chemistry, University of Delhi, Delhi-110007, India
[b] Institute of Nano Medical Sciences, University of Delhi, Delhi-110007, India

ARTICLE INFO

Keywords:
Nanobiosensor
Graphdiyne
Liver cancer
Annexin A2
Nanosheets

ABSTRACT

Herein, we report synthesis of 2D few-layered transparent hydrogen substituted graphdiyne (HsGDY) nanosheets and explored its electrochemical characteristics for the first time to develop a nano-interface for cancer biomarker detection [liver cancer (LC) biomarker; ANXA2]. The semiconducting HsGDY (band gap; 1.98 eV) contains considerable number of sp and sp^2 hybridised π-electrons with abundant hierarchical pores, thus reveals a negative peripheral charge and high surface area respectively, making it competent to immobilize mass anti-ANXA2 antibodies. The nano-interface platform is fabricated through electrophoretic deposition of HsGDY onto indium tin oxide (ITO) coated glass substrate (50V, 60s) with subsequent immobilization of anti-ANXA2 biomolecules and bovine serum albumin (BSA) to minimize non-specific binding. The pristine HsGDY and fabricated electrodes were characterized using spectroscopic, microscopic, zetasizer, surface area and pore size analyzer as well as electrochemical techniques. The electrochemical response of fabricated HsGDY nano-interface based biosensing platform (BSA/anti-ANXA2/HsGDY/ITO) is investigated via cyclic voltammetry (CV) and differential pulse voltammetry (DPV) techniques, which covers a wider linear detection range in between 0.01 fg mL^{-1} to 1000 ng mL^{-1} along with an exceptional sensitivity of 13.8 μA [log (ng mL^{-1})]$^{-1}$ cm^{-2} and 2.8 μA [log (ng mL^{-1})]$^{-1}$ cm^{-2} via CV and DPV techniques, respectively. This developed biosensor has the ability for unprecedented ultralow level i.e., upto 3 molecules of ANXA2 cancer biomarker detection. Moreover, the obtained electrochemical results show excellent correlation with the concentration of ANXA2 cancer biomarker present in LC patients obtained through enzyme linked immunosorbent assay (ELISA) technique.

1. Introduction

Covalent organic frameworks are highly ordered structures due to covalent network of organic monomers, creating a robust backbone and owns permanent porosity which imparts large surface area and high adsorption potentials. The porous structure unveils ordered channels allowing rapid ion and charge transfer. Henceforth, finds applications in gas separation and adsorption, energy storage devices, catalysis, drug delivery, sensors, etc. (Chen et al., 2020; Kumar et al., 2021a; Wu and Yang, 2017) Recently, an interlinked organic framework enriched with π-electrons i.e., HsGDY, is introduced as a rising star with high conjugation and polymerized through multiple units of 1,3,5-triethynylbenzene (TEB). It comprises of repeating structural units of a big hexagonal ring assembled by 42 carbon atoms, each unit composed of 6 benzene rings (sp^2 hybridised) interlinked by diacetylenic linkages (-C≡C–C≡C-; sp hybridised), thereby furnishing it with uniform in-plane cavities distributed throughout the structure (He et al., 2017; Wang et al., 2019). This synthetic carbon allotrope differ in structure and properties from other carbon allotropes due to presence of sp^2 as well as sp hybridised carbon atoms which leads to inhomogeneous π-bondings, thus ensuing natural band gap in semiconducting range, a favourable condition for nanoelectronics unlike graphene, which has a zero-band gap (Chen et al., 2015; Huang et al., 2018). Additionally, it is endowed with high intrinsic carrier mobility (upto 10^5 cm^2 V^{-1} s^{-1}) due to the presence of dirac points and cones; thus suggesting high conductivity reaching upto 10^3 S m^{-1} (Huang et al., 2018). The presence of sp hybridised carbon atoms results in more favourable and stronger interaction of biomolecules with GDY and its counterparts as compared

* Corresponding authors.
E-mail addresses: acbrdu@hotmail.com (R. Chandra), suveendev@gmail.com (S. Kumar).

https://doi.org/10.1016/j.bios.2022.114433
Received 12 December 2021; Received in revised form 2 May 2022; Accepted 25 May 2022
Available online 30 May 2022

to graphene (Parvin et al., 2017). Furthermore, the hierarchical pores provide additional pathway for facile diffusion of ions perpendicular to the molecular plane; unlike the steric hindrance caused in graphene due to sp^2 hybridised carbons (Gong et al., 2020). Thus, these sp-circumferenced cavities provide tunnels for electrons hopping, high surface area and strong adsorption ability for loading of biomolecules, that help in amplifying the signal to noise ratio of electrochemical signals and lead to enhanced sensitivity and quick response (He et al., 2017; Li et al., 2020; Parvin et al., 2017). Thus, HsGDY appears as an expedient support for development of electrochemical biosensors. Therefore, in this work we have explored the electrochemical properties of HsGDY towards fabrication of a biosensing platform for cancer detection.

Cancer characterized by aberrant cell growth in an unregulated manner, is the leading cause of death worldwide with third position occupied by LC, reporting 8,30,000 deaths in 2020 (Kumar et al., 2019; "WHO Fact sheet," 2021). Various factors such as cirrhosis, viral hepatitis, aflatoxin consumption triggers the risk of LC (Dasgupta et al., 2020). Conventionally, the detection methods of LC include ultrasonography, CT-scan, hepatic angiography, laparoscopy and biopsy (Bialecki and Di Bisceglie, 2005; Marrero et al., 2018). However, lack of sensitivity, radiation exposure, false results, contrast injury, appearance of large and mimic nodules, prolonged time and instrument sophistication along with highly distressing nature of biopsy, limits their application in LC detection (Atiq et al., 2017; Bialecki and Di Bisceglie, 2005). In this context, electrochemical biosensors represent a user-friendly and minimal invasive platform which offers high sensitivity, accuracy and requires less time. Various LC biomarkers have been explored such as AFP, DCP, GPC3, AFU, etc., however they suffer from low sensitivity and specificity at optimal cut-off values and influenced by other medical conditions, which leads to false results thereby, deviating from accuracy (Bialecki and Di Bisceglie, 2005; Sun et al., 2013). In this regard, an underexplored minimal invasively secreted biomarker, i.e., Annexin A2 (ANXA2; molecular weight 36 kDa) delivers excellent diagnostic parameters (sensitivity: 80.4–100%; specificity: 84–91% and negative-predictive value: 86–100%) for LC detection. Its over-expression is recorded in early stage LC patients with a cut-off value of 18 ng mL^{-1}, which rises above 500 ng mL^{-1} in LC patients (Chauhan et al., 2021; El-Abd et al., 2016). Thus, quantifying the serological concentration of ANXA2 provide an accurate and minimal invasive approach to detect LC.

Herein, we synthesized few-layered HsGDY nanosheets and utilized it as a nano-interface to fabricate a platform for ANXA2 detection. The developed biosensor showed excellent analytical parameters with the ability for ultralow sensing of 3 molecules of ANXA2. Further, the results obtained for electrochemical response for serum samples of LC patients were correlated with ELISA, indicating high accuracy of the assay. To the best of our knowledge, this is the first report towards use of HsGDY as nano-interface for the development of biosensor for cancer detection.

2. Materials and methods

2.1. Chemicals and biomolecules

1,3,5-Triethynylbenzene (TEB; $C_{12}H_6$), N-(3-dimethylaminopropyl)-N-ethylcarbodiimide hydrochloride (EDC; $C_8H_{17}N_3$) and N-hydroxysuccinimide (NHS; $C_4H_5NO_3$) were purchased from Sigma-Aldrich. Hydrochloric acid (HCl), N, N-dimethylformamide (DMF; C_3H_7NO) and magnesium nitrate hexahydrate ($Mg(NO_3).6H_2O$) were procured from Fisher Scientific. Copper foil (0.1 mm, 99% pure) was purchased from Loba Chemie Pvt. Ltd. Sodium hydroxide (NaOH) and bovine serum albumin (BSA) were obtained from SRL Pvt. Ltd. Acetone (C_3H_6O) and pyridine (C_5H_5N) were purchased from Rankem Laboratory Reagent. Sodium dihydrogen phosphate dihydrate ($NaH_2PO_4.2H_2O$), disodium hydrogen phosphate dihydrate ($Na_2HPO_4.2H_2O$), potassium hexacyano ferrate (II) trihydrate ($K_4Fe(CN)_6.3H_2O$), potassium hexacyano ferrate (III) ($K_3Fe(CN)_6$) and sodium chloride (NaCl) were procured from Merck Life Science Pvt. Ltd. Human/mouse/rat monoclonal Annexin A2 monoclonal antibody (anti-ANXA2) and recombinant human Annexin A2 protein (ANXA2) biomolecules were acquired from R & D Systems. Human Annexin A2 ELISA kit was purchased from Bioassay Technology Laboratory. The biomolecules were diluted using PBS buffer (pH = 7.0) composed of 0.2 M $NaH_2PO_4.2H_2O$, 0.2 M $Na_2HPO_4.2H_2O$, 0.9% NaCl in deionized water and stored at 4 °C till further use. All the chemicals were of analytical grade and were used without any purification.

2.2. Instrumentation

The structure and purity of pristine HsGDY was examined using X-ray diffraction (XRD; Rigaku miniflex 600) studies by using Cu-kα beam having wavelength (λ) of 0.15406 nm and nuclear magnetic resonance (NMR; Bruker Topspin 4.0.8) spectroscopy. Further, to study the modification of bonds and functional groups in the synthesized material and fabricated bioelectrodes, Fourier transform-infrared spectroscopy (FT-IR; Shimadzu IR Affinity 1S) studies were performed. The morphology of HsGDY and fabricated electrodes was analysed through scanning electron microscopy (SEM; JEOL JSM 6610LV, Japan) and transmission electron microscopy (TEM; TALOS S Thermo Scientific). To obtain the band gap of HsGDY, UV-Vis (Perkin Almer) spectrum was recorded. The surface properties of HsGDY were investigated through surface area and pore size analyzer (Micromeritics Gemini V). The zeta potential of HsGDY was measured using zetasizer (Zetasizer nano-ZS). The concentration of ANXA2 in serum samples of LC patients was investigated using ELISA plate reader (Biotek 800 TS microplate reader). The electrochemical characterization was investigated through cyclic voltammetry (CV) and differential pulse voltammetry (DPV) techniques using Autolab Potentiostat Galvanostat (AUT204, Netherlands). The studies were conducted in phosphate buffer saline (PBS) of pH = 7.0 composed of 0.2 M $NaH_2PO_4.2H_2O$, 0.2 M $Na_2HPO_4.2H_2O$ and 0.9% NaCl in deionized water, containing 5×10^{-3} M of potassium ferri/ferrocyanide $[Fe(CN)_6]^{3-/4-}$ as redox couple. For the setup, a three-electrodes system consisting of indium tin oxide (ITO) coated substrate as working electrode, platinum (Pt) as counter electrode and silver/silver chloride (Ag/AgCl) as reference electrode was used. All the electrochemical studies were conducted in triplicate (n = 3).

2.3. Collection and processing of serum samples

The collection and processing of serum samples was accomplished at National Liver Disease Biobank, Institute of Liver and Biliary Sciences, New Delhi, India. All the samples of LC patients were obtained by following the prescribed protocol of the biobank. Along with this, an approval was obtained from Institutional Ethical Committee (IEC) and Animal Ethics Committee (Ref. No: CHEM/2238) of Department of Chemistry, University of Delhi, India to conduct further studies using these biological samples. The samples were collected in pre-sterilized vials followed by leaving the samples undisturbed for 20 min to allow clotting of blood. Further, the samples were centrifuged and the supernatant containing serum was used to conduct further experiments.

2.4. Synthesis of hydrogen substituted graphdiyne (HsGDY)

HsGDY was synthesized by following previously reported method by He *et al.* with slight modifications. Briefly, 20–25 pieces of Cu foils (2.5 cm × 2 cm) were firstly pre-treated by sonicating serially in HCl, acetone and ethanol to remove the oxidized layer of Cu and dried in an inert atmosphere at 60 °C. Then, the foils were added to 50 mL pyridine in a two-necked round bottom flask and a solution of 100 mg TEB in 50 mL pyridine was added dropwise with the help of dropping funnel. The solution was kept for stirring (300 rpm) at 60 °C for 72 h. After the completion of reaction, HsGDY films grown on Cu foils along with the

brown-colored powder were taken out and washed with acetone, DMF and ethanol sequentially and kept for drying in an oven at 60 °C for 24 h. The films from Cu foils were peeled off by keeping them in a solution of 2 M HCl solution for 30 min and washing them with 4 M NaOH and distilled water until pH becomes neutral. Finally, washed the films with ethanol and kept for drying. The films along with HsGDY powder were grounded finely using mortar and pestle and used for further studies.

2.5. Fabrication of biosensing platform

For the deposition of HsGDY onto ITO substrate, electrophoretic deposition (EPD) technique was employed. For this purpose, a two-electrodes system was utilized comprising of ITO as cathode and Pt as anode, both standing 1 cm apart from each other. Thereafter, ~6 mL freshly sonicated solution of HsGDY in DMF (1 mg mL^{-1}) was used and 10–20 μL of $Mg(NO_3)_2.6H_2O$ solution in DMF (50 mg mL^{-1}) was added. An optimized DC potential of 50 V was applied for 90 s to obtain brown-colored films on the conducting ITO substrate. The shape of ITO electrodes was rectangular with the active surface area modified using HsGDY is 0.5 cm × 0.5 cm, i.e., 0.25 cm^2. There is no dissimilarity in the shape of different electrodes, all electrodes were prepared under the identical conditions covering similar 0.25 cm^2 of active surface area. Next, the fabricated platform (HsGDY/ITO) was then washed using PBS to remove any unbound molecules. Next, a solution of EDC, NHS and anti-ANXA2 (50 μg mL^{-1}) was prepared in 1:1:2 ratio and 30 μL of this activated solution was drop-cast onto HsGDY/ITO platform and incubated at 4 °C. The platform (anti-ANXA2/HsGDY/ITO) was washed thrice with 30 μL of PBS and lastly, 20 μL of 2 mg dL^{-1} BSA was drop-cast to minimize the binding with non-specific sites. The fabricated platform (BSA/anti-ANXA2/HsGDY/ITO) was washed using PBS and kept at 4 °C for further use.

3. Results and discussion

3.1. Structural and morphological properties of HsGDY

The structure and purity of the TEB monomer was ensured by ^{1}H-NMR and ^{13}C-NMR spectra as discussed in supplementary file (Figs. S1 and S2). The solid state ^{13}C-NMR of HsGDY was recorded to inspect the different types of carbons present in product and the spectrum is shown in Fig. 1 (A). The peaks at δ = 136.7 ppm and δ = 123.3 ppm are ascribed to two kinds of C (sp^2) aromatic carbons attached to H and C (sp^2) atoms respectively, while those at δ = 81.1 ppm and δ = 76.6 ppm correspond to other two kinds of linear C (sp) attached to C (sp^2) and C (sp) carbons, respectively, thus confirming the four different types of carbon having sp^2 as well as sp hybridisation (Pavia et al., 2010). Further, XRD pattern of HsGDY [Fig. 1 (B)] shows a broad peak centred at approximately 24.03° congruent to (002) plane of amorphous carbon materials with an interlayer distance of 0.36 nm, which is in excellent harmony with computed values, thus accomplishing successful synthesis of HsGDY (Wang et al., 2019). The broadness of peak indicates the small crystalline domain size along with formation of 2D thin nanosheets, arising due to conformational fluctuations of HsGDY at mesoscopic scales (He et al., 2017; Holder and Schaak, 2019). Successively, to investigate the functionalities present on HsGDY, FT-IR spectrum of TEB and HsGDY was recorded. Fig. 1 (C) clearly shows the low intensity peaks in between 2250 and 2110 cm^{-1} corresponding to C≡C bond stretch with the peaks between 1577 and 1388 cm^{-1} due to aromatic region of C=C stretch and aromatic C–H out of plane bending at 880 cm^{-1} present in both precursor and synthesized product. The characteristic peak of ≡C–H at 3271 cm^{-1} is observed in TEB, however, absence of this sharp peak in HsGDY indicates successful synthesis of the product.

The morphology of pristine HsGDY was examined through SEM and TEM. The SEM images of HsGDY film on glass substrate and powder [Fig. S3 (A, B)] shows smooth plain surface and bulk rough nanosheets morphology, respectively. Further, few-layered thin sheets (lighter

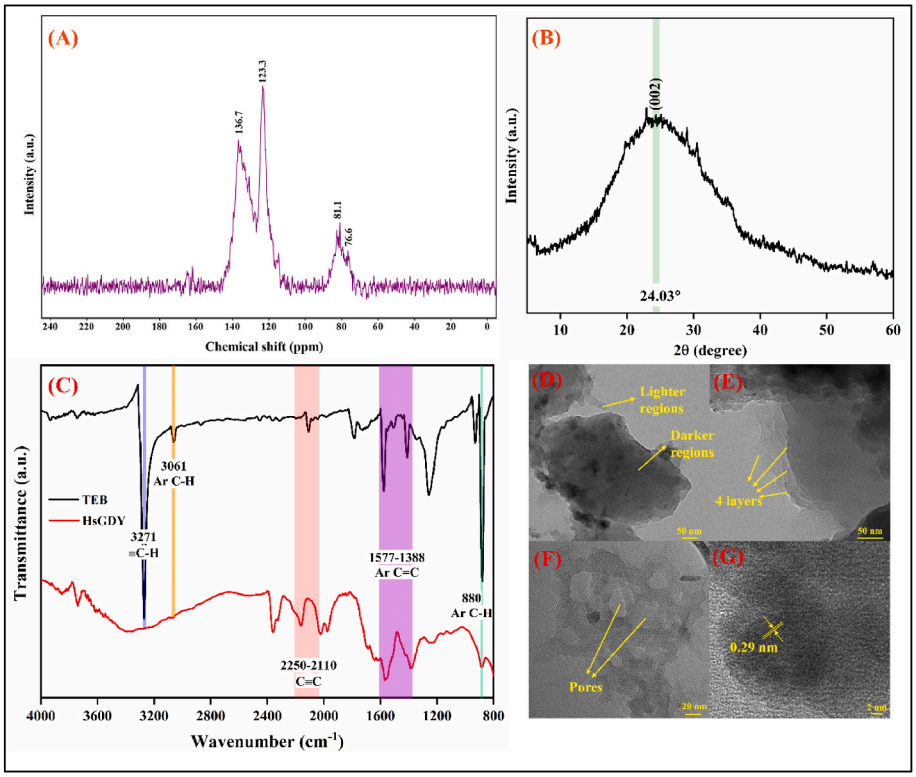

Fig. 1. (A) Solid state ^{13}C-NMR of pristine HsGDY, (B) XRD pattern of HsGDY, (C) FT-IR spectra of TEB and HsGDY, TEM images showing (D) nanosheets morphology with darker and lighter regions, (E) few layers, (F) pores and (G) HR-TEM of HsGDY.

regions) and stacked sheets one over another (darker regions) in Fig. 1 (D, E) are visible in TEM images. The appearance of sheets can be correlated to the broadness of peak in XRD spectrum, indicating successful formation of thin 2D nanosheets (Holder and Schaak, 2019). Furthermore, porous structure can be seen in Fig. 1 (F) with visible lattice fringes in HR-TEM [Fig. 1 (G)] corresponding to interlayer spacing of 0.29 nm. These findings clearly support the successful synthesis of few-layered porous HsGDY nanosheets.

The optical images of HsGDY films are shown in Fig. 2 (A-H). A thin layer of HsGDY grown on copper foils is shown in Fig. 2 (A) which gets peeled off in HCl solution [Fig. 2 (B)]. Using wet stripping method, $FeCl_3$ was used to transfer the films on various substrates like whatmann filter paper, glass slide, etc. as shown in Fig. 2 (C). The dried films [**inset; Fig. 2 (D)**] with a single layer holding through forceps is shown in Fig. 2 (D) and stored in vial filling it completely, showing large volume occupancy of few mg of sample [Fig. 2 (E)]. The large area yellow-colored HsGDY film was obtained on glass slide, largest covering an area of 2.5 × 1.5 cm^2 with high transparency as shown in Fig. 2 (F, G, H). These results are in accordance with the successful formation of 2D transparent nanosheets of HsGDY having very low density.

3.2. Surface, charge and electronic properties of HsGDY

To get an insight into surface of HsGDY, nitrogen adsorption-desorption studies were performed. The mean pore size was recorded as 7.8 nm with Brunauer-Emmett -Teller (BET) surface area as 26 $m^2 g^{-1}$. The adsorption-desorption isotherms and pore size distribution are shown in Fig. 3 (A, B), representing hierarchical pore distribution with combination of mesopores and micropores. Further, to measure the electronic properties, the UV–Vis spectrum of synthesized HsGDY was recorded and shown in Fig. 3 (C). A broad band centred at 548 nm was observed and after Kubelka-Munk transformation, band gap was calculated as 1.98 eV using Tauc's plot by following the relation $\alpha \propto (h\upsilon\text{-}Eg)^{1/2}/h\upsilon$, suggesting the semiconducting behaviour of HsGDY (Zhang et al., 2020). Thus, HsGDY provide a suitable substrate for development of nanoelectronic devices. The peripheral charge on HsGDY was studied using zetasizer and recorded as −12.06 mV, which is highly negative than other graphene analogues, suggesting greater number of negatively charged π-electrons present in HsGDY (Vannozzi et al., 2021). Thus, it functions as an efficient matrix for immobilization of mass antibodies through their positively charged amine groups, resulting in the fabrication of an efficient biosensing platform.

3.3. Characterization of fabricated electrodes

The successful immobilization of anti-ANXA2 antibodies onto HsGDY/ITO platform was confirmed using FT-IR spectroscopy studies. The FT-IR spectra of HsGDY/ITO and anti-ANXA2/HsGDY/ITO electrodes (Fig. S4) shows the peaks around 2330 cm^{-1} due to C≡C stretch and in the region 1463-1386 cm^{-1} due to aromatic C═C bonds stretch. However, in anti-ANXA2/HsGDY/ITO, additional band at 3330-3300 cm^{-1} appears due to the N–H stretching in antibodies with a peak at 1641 cm^{-1} due to overlapping of amide I (C═O stretch) and amide II (N–H bend) bands, along with the corresponding C–N peak at 1076 cm^{-1}, confirming the successful immobilization of anti-ANXA2 antibodies onto HsGDY framework (Pavia et al., 2010). Further, to accord the changes in morphology upon anti-ANXA2 immobilization onto HsGDY/ITO electrode, SEM images were recorded as shown in Fig. S5 (A-D). The SEM image of HsGDY/ITO electrode clearly depicts deposition of HsGDY with slight rough surface [Fig. S5 (A, B)] while that of anti-ANXA2/HsGDY/ITO electrode shows spotted surface with globular antibodies, exposing a shinier and fully covered smooth surface [Fig. S5 (C, D)], thus confirming successful immobilization of anti-ANXA2 (Das et al., 2015; Kumar et al., 2021b).

3.4. Electrochemical characterization and response studies

To study the electrochemical behaviour at different steps of electrode surface modification, CV curve is recorded (potential range: −0.8V to +0.8V, scan rate: 50 mV s^{-1}) [Fig. 3 (D)]. The anodic peak current (I_{pa}) of ITO was recorded as 463.2 μA. The increased I_{pa} (529.4 μA) after deposition of HsGDY onto ITO is evident due to numerous ion transporting tunnels in HsGDY that amplifies the electrochemical signal (Gong et al., 2020). The I_{pa} lowers after anti-ANXA2 (518.1 μA) and BSA (513.6 μA) immobilization due to sequential formation of insulating biomolecules layers, thus confirming the successful fabrication of BSA/anti-ANXA2/HsGDY/ITO biosensor(Jain et al., 2021). Furthermore, effect of scan rate on BSA/anti-ANXA2/HsGDY/ITO electrode demonstrate diffusion-controlled and quasi-reversible interfacial electron transfer kinetics and results are summarized in supplementary file [Fig. S6 (A-C)](Chaudhary et al., 2021).

Next, to monitor the time required for complete interaction of ANXA2 with BSA/anti-ANXA2/HsGDY/ITO immunoelectrode and confirm the absolute formation of antibody-antigen immunocomplex, response time studies were conducted by recording the changes in

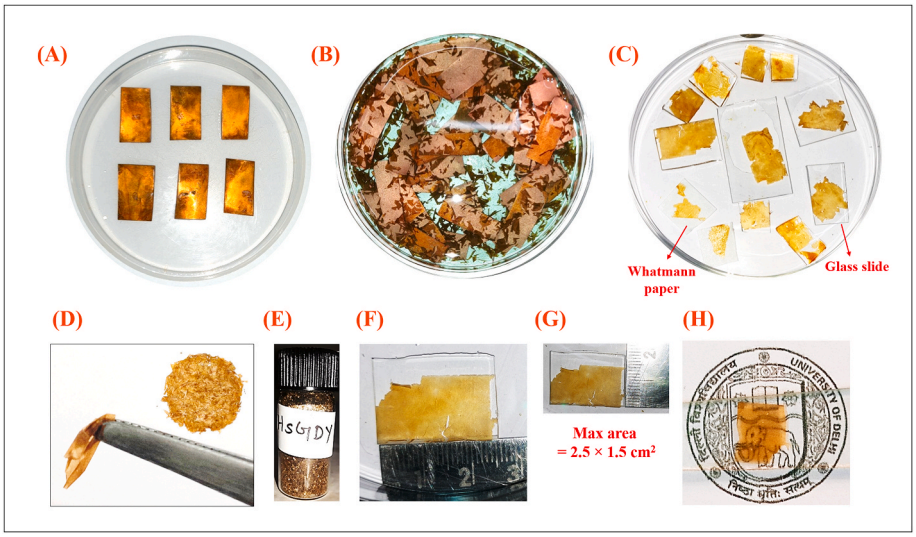

Fig. 2. Optical images of HsGDY films (A) grown on copper foils, (B) peeled off in HCl solution, (C) transferred onto various substrates (whatmann filter paper, glass slide), (D) single film held by forceps; inset: dried scrapped HsGDY films, (E) light weight few mg HsGDY filling full vial (F, G) measuring large area 2.5 × 1.5 cm^2 and (H) showing high transparency.

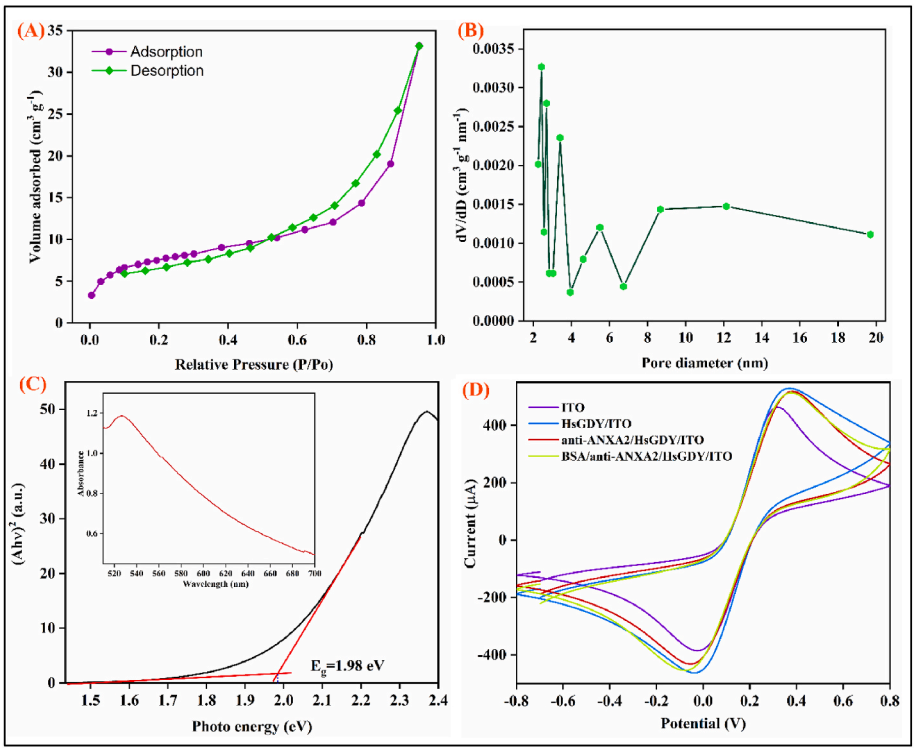

Fig. 3. (A) N_2 adsorption-desorption isotherm of HsGDY, (B) pore size distribution, (C) Tauc plot obtained from UV–Vis spectra of HsGDY, inset: UV–Vis absorption spectrum of HsGDY and (D) CV of ITO, HsGDY/ITO, anti-ANXA2/HsGDY/ITO and BSA/anti-ANXA2/HsGDY/ITO electrodes.

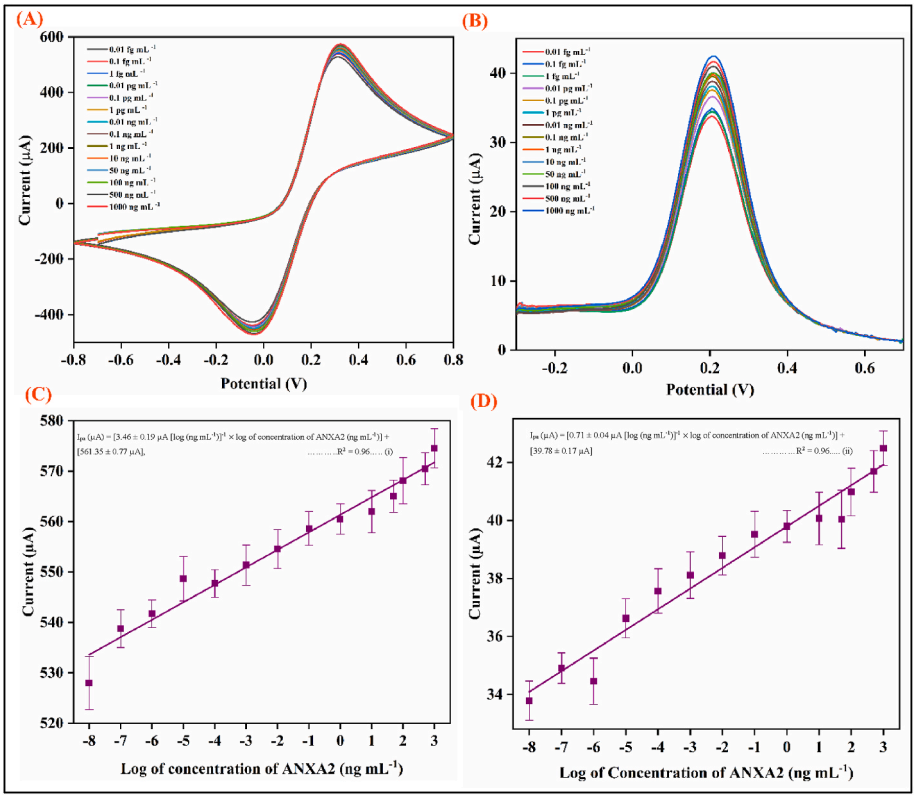

Fig. 4. Electrochemical response of BSA/anti-ANXA2/HsGDY/ITO as a function of increasing concentrations of ANXA2 (0.01 fg mL^{-1}-1000 ng mL^{-1}) through (A) CV and (B) DPV techniques and calibration plot of magnitude of anodic peak current against log of concentration of ANXA2 (0.01 fg mL^{-1}-1000 ng mL^{-1}) through (C) CV and (D) DPV techniques.

anodic peak current periodically after addition of ANXA2 antigen. It is observed that the anodic peak current increases till a maximum is reached at 20 min, afterwards the curve flattens and a constant response was obtained (data not shown). Therefore, an incubation period of 20 min was provided after each addition of ANXA2 concentration. Following this, the electrochemical response of fabricated immunoelectrode BSA/anti-ANXA2/HsGDY/ITO was investigated against ANXA2 using CV (potential range: −0.8V to +0.8V, scan rate: 50 mV s^{-1}) and DPV (potential range: −0.3 V to +0.7 V) techniques [Fig. 4 (A, B)] at varying concentration from 0.01 fg mL^{-1} to 1000 ng mL^{-1} which shows a linear increasing fashion with positive inclination and governed by **eq. (i) and (ii)** [Fig. 4 (C, D)], attributed to electroactive cysteine residues in ANXA2 augmenting the current response (Madureira and Waisman, 2013). Along with this, HsGDY endowed with transfer canals facilitate hopping of electrons across the electrode-electrolyte interface by acting as electron acceptor and donor species, thus intensifies the electron transfer process and assist in amplifying the electrochemical signals (Gong et al., 2020; Zhao et al., 2018), thus achieving wider LDR of 0.01 fg mL^{-1}-1000 ng mL^{-1} and LOD of 0.01 fg mL^{-1}. At this remarkable LOD, the biosensor could sense even 3 molecules of ANXA2 (calculations given below), thus detecting an ultralow concentration of ANXA2. Moreover, the porous framework of HsGDY act as excellent matrix owing to its strong non-covalent interactions with biomolecules due to the negative surface charge that assist in adsorbing mass anti-ANXA2 antibodies, thus attaining excellent sensitivity of 13.8 μA [log (ng mL^{-1})]$^{-1}$ cm^{-2} and 2.8 μA [log (ng mL^{-1})]$^{-1}$ cm^{-2} through CV and DPV techniques, respectively. Henceforth, the proposed HsGDY biosensor shows excellent biosensing parameters to efficiently detect LC. A comparative analysis showing analytical parameters of various biosensors for LC detection is shown in Table 1.

Calculation of number of molecules in ANXA2 at LOD of 0.01 fg mL^{-1}:

Molecular weight of ANXA2 = 36 kDa or 36 × 10^3 g mol^{-1}

Concentration (strength) of ANXA2 solution at LOD = 0.01 fg mL^{-1} or 10^{-14} g L^{-1}

Thus, molarity of solution

= strength/ molecular weight

= 10^{-14} g L^{-1}/ 36 × 10^3 g mol^{-1}

= 2.77 × 10^{-19} mol L^{-1}

Number of molecules of ANXA2 in this concentration

= Molarity × Avogadro number

= 2.77 × 10^{-19} mol L^{-1} × 6.022 × 10^{23} molecules mol^{-1}

= 1.6 × 10^5 molecules L^{-1}

So, number of molecules in 1 L or 10^6 μL of solution = 1.6 × 10^5 molecules.

Therefore, Number of molecules in 20 μL of solution

= 1.6 × 10^5 molecules × 20 μL/ 10^6 μL

= 3.2 molecules

~3 molecules per 20 μL

Hence, 20 μL of 0.01 fg mL^{-1} solution contains ~ 3 molecules of ANXA2.

3.5. Control, Interferent, Reproducibility and Shelf life studies

To validate the changing current upon binding of ANXA2 to BSA/anti-ANXA2/HsGDY/ITO immunoelectrode, a control experiment was set up by using HsGDY/ITO electrode and thereafter, electrochemical response was recorded by addition of increasing ANXA2 concentrations. It can be seen from Fig. 5 (A) that no substantial difference in anodic peak current was observed. Therefore, it is inferred that the development of immunocomplex is entirely responsible for variations in peak current values during electrochemical response experiment. Further, to evaluate the selectivity of the fabricated platform against ANXA2, different interferents (cTn-I, CYFRA-21-1, CKAP4, SAA, urea, ascorbic acid) present in human serum were sequentially added to record the electrochemical response of BSA/anti-ANXA2/HsGDY/ITO immunoelectrode. As evident from Fig. 5 (B), current changes are observed only after addition of ANXA2 and afterwards, no significant variation is observed upon addition of interferents, yielding average percent relative standard deviation (%RSD) of ~0.3%. Thus, the developed biosensing platform showed high selectivity towards ANXA2 detection. Next, to validate the reproducibility of the immunosensors, six different electrodes (BSA/anti-ANXA2/HsGDY/ITO) were fabricated under similar experimental conditions and electrochemical response was recorded via CV technique. The obtained anodic peak currents of different electrodes are represented as bar graph in Fig. S7. It was found that average %RSD of anodic peak current of different immunoelectrodes was ~1.0%, indicating high reproducibility of the fabricated biosensing electrode. Furthermore, the shelf life of fabricated BSA/anti-ANXA2/HsGDY/ITO electrode was recorded via CV technique after every 7 days. It was found that the electrochemical response retained its 98% value of its peak current till 35 days, thereafter it started declining and reached upto 94% and 92% till 42 and 49 days (Fig. S8). Hence, our fabricated working electrode, i.e., BSA/anti-ANXA2/HsGDY/ITO exhibits a shelf life of 35 days.

3.6. Real sample analysis

The concentration of ANXA2 in serum samples of 4 LC patients was quantified using ELISA. The assay was performed in triplicate for

Table 1
Comparative table showing analytical parameters of various biosensors along with the present work for LC detection.

Detection technique	Biomarker	Material used	LDR	LOD	Sensitivity	Response time	Ref.
DPV	AFP	Au	0.5–80 ng mL^{-1}	0.25 ng mL^{-1}	–	30 min	Ding et al. (2009)
DPV	GP73	Nafion	3 × 10^{-4}-6 ng mL^{-1}	1 × 10^{-4} ng mL^{-1}	–	90 min	Zhang et al. (2018)
CA	AFP	PANI-BSA-Ag	0.01–1 & 1–10 ng mL^{-1}	4.7 × 10^{-3} ng mL^{-1}	–	60 min	Amarnath and Sawant (2020)
DPV	AFP	PEG/Au/PANI	1 × 10^{-5}–1 ng mL^{-1}	7 × 10^{-6} ng mL^{-1}	–	60 min	Hui et al. (2016)
CV	ANXA2	MWCNT	0–60 ng mL^{-1}	–	1.805 μA mL ng^{-1} cm^{-2}	15 min	Chauhan et al. (2021)
DPV	ANXA2	HsGDY	10^{-8}-1000 ng mL^{-1}	10^{-8} ng mL^{-1}	2.8 μA [log (ng mL^{-1})]$^{-1}$ cm^{-2}	20 min	**Present work**
CV	ANXA2	HsGDY	10^{-8}-1000 ng mL^{-1}	10^{-8} ng mL^{-1}	13.8 μA [log (ng mL^{-1})]$^{-1}$ cm^{-2}	20 min	

(Abbreviations: AFP: α-feto protein, ANXA2: Annexin A2, CA: Chronoamperometry, CV: Cyclic voltammetry, DPV: Differential pulse voltammetry, GP73: Golgi protein 73, LDR: Linear detection range, LOD: Limit of detection, MWCNT: Multi-walled carbon nanotube, PANI: Polyaniline, PEG: Polyethylene glycol).

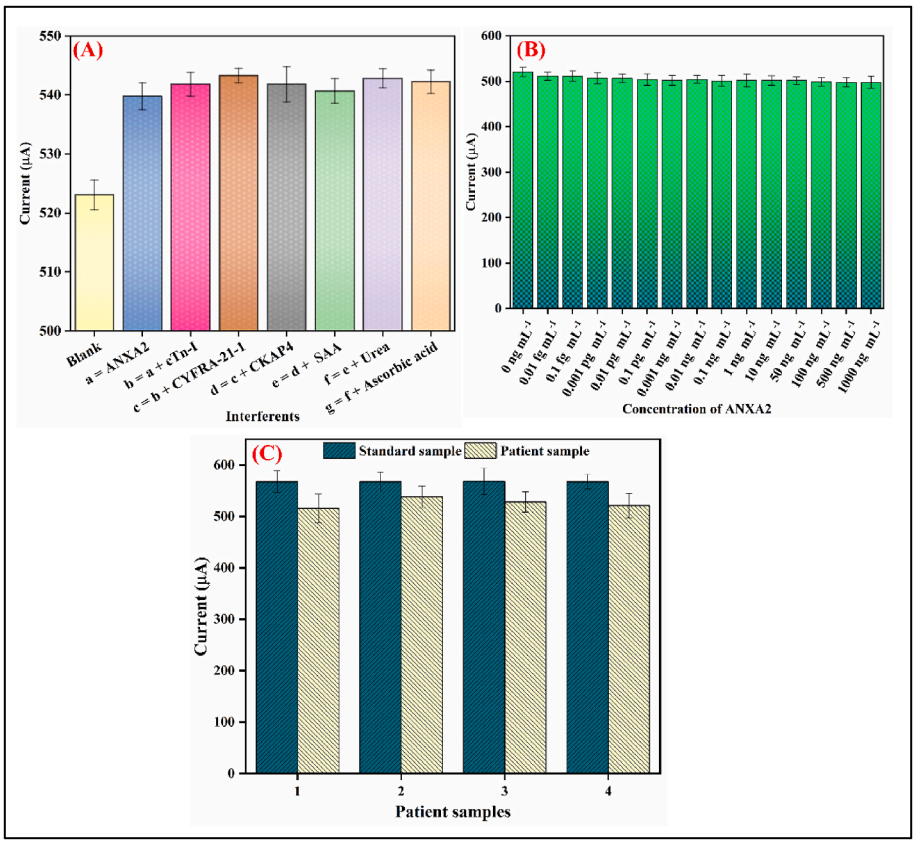

Fig. 5. (A) Control studies showing electrochemical response of HsGDY/ITO against increasing concentrations of ANXA2 (0.01 fg mL^{-1}-1000 ng mL^{-1}), (B) interferent studies conducted using various analytes present in human serum along with ANXA2 and (C) bar graph showing comparison of current obtained through CV of standard and LC patient samples.

standard solutions and serum samples using microtiter 96 wells plate pre-coated with anti-ANXA2 by following all the steps according to the provided protocol. Thereafter, the fabricated biosensor (BSA/anti-ANXA2/HsGDY/ITO) was used to record the electrochemical response of the serum samples through CV. The obtained results along with the patients' characteristics are tabularized in Table S1 and presented in bar graph as shown in Fig. 5 (C). It is unambiguous that a rational average % RSD of ~5% between the current response of standard solutions and serum samples is obtained, signifying high accuracy of the fabricated biosensor towards its application in LC detection.

3.7. Assay precision and accuracy

To validate the assay precision, intra assay standard deviations (SD) and coefficients of variance (CoV) were measured using both CV and DPV techniques at different standard concentrations of ANXA2 viz, 0.01 fg mL^{-1}, 0.01 pg mL^{-1}, 0.01 ng mL^{-1}, 1 ng mL^{-1}, 10 ng mL^{-1}, 100 ng mL^{-1} and 1000 ng mL^{-1}. These measurements were conducted by repeating the experiments in triplicate (n = 3) and a response of three consecutive measurements were recorded after a given optimized incubation time on a single day. Thus, an average of 3 × 3, i.e., nine observations were considered to calculate the CoV. The values of SD and CoV are tabulated in Table S2 with the overall mean intra-assay CoV (%) as 0.06% via CV and 0.21% via DPV techniques. The obtained values of mean intra-assay CoV (%) results indicate high precision of assay for clinical applications. Further, in order to validate the results obtained using serum samples of LC patients, statistical analysis using students's *t*-test and F-test were performed by comparing their response against the electrochemical response of blank electrodes (BSA/anti-ANXA2/HsGDY/ITO). For this purpose, average mean of anodic peak current of four electrodes (BSA/anti-ANXA2/HsGDY/ITO) before and after addition of serum samples were taken and each measurement was repeated in triplicate (n = 4 × 3). The paired *t*-test presented high statistical difference between the two currents within a confidence interval of 99.9% ($p <<< 0.001$), thus demonstrating that the two currents were reasonably different not due to random errors. Furthermore, F-test also demonstrated large gap between the electrochemical response of blank electrodes before and after addition of serum samples with $p <<< 0.001$. The results tabulated in Table S3 indicate that our fabricated immunosensor has the ability to detect ANXA2 in the serum samples of LC patients with high accuracy.

4. Conclusions

In this work, we report development of 2D few-layered transparent semi-conducting HsGDY nano-interface based platform for LC biomarker (ANXA2) detection. The hierarchical porous structure and negative peripheral charge on HsGDY helps to immobilize mass antibodies and presence of canals for electron hopping helps in achieving excellent biosensing parameters with wide linear detection range of 0.01 fg mL^{-1}-1000 ng mL^{-1} with exceptional sensitivity of 13.8 μA [log (ng mL^{-1})]$^{-1}$ cm^{-2} and 2.8 μA [log (ng mL^{-1})]$^{-1}$ cm^{-2} via CV and DPV techniques, respectively. This fabricated biosensing platform has the ability for unprecedented ultralow level i.e., upto 3 molecules of ANXA2 cancer biomarker detection. Thus, HsGDY dominates graphene in terms of owning inherent band gap along with having high conductivity and forming transparent films. Therefore, semiconducting HsGDY holds enormous potential for its application as expedient nano-interface for development of efficient biosensor for various diseases detection as well as flexible wearables and nanoelectronics.

CRediT authorship contribution statement

Dipti Chauhan: Formal analysis, Investigation, Resources, Writing – original draft. **Yogesh Kumar:** Formal analysis, Investigation. **Ramesh Chandra:** Writing – review & editing. **Suveen Kumar:** Conceptualization, Methodology, Supervision, Validation, Writing – review & editing.

Declaration of competing interest

The authors declare that they have no known competing financial interests or personal relationships that could have appeared to influence the work reported in this paper.

Acknowledgements

Authors thank Vice Chancellor, University of Delhi for providing infrastructure and other facilities. DC and YK thank UGC fellowship (191620082661 and 99/CSIRNETJUNE2019, respectively) for financial assistance. SK acknowledges DST for INSPIRE-Fellowship (DST/INSPIRE/04/2017/001336) and Institute of Eminence, University of Delhi (IoE/2021/12/FRP) for financial research support. Authors thank Dr. Birendra Kumar Yadav, Biobank Manager, NLDB, ILBS, Delhi, India for providing serum samples. Authors also express gratitude to University Science Instrumentation Centre (USIC) and sophisticated analytical instrumentation facility (SAIF), AIIMS for providing the necessary instrumentation.

Appendix A. Supplementary data

Supplementary data to this article can be found online at https://doi.org/10.1016/j.bios.2022.114433.

References

Amarnath, C.A., Sawant, S.N., 2020. Polyaniline based electrochemical biosensor for α-fetoprotein detection using bio-functionalized nanoparticles as detection probe. Electroanalysis 32, 2415–2421. https://doi.org/10.1002/elan.202060219.

Atiq, O., Tiro, J., Yopp, A.C., Muffler, A., Marrero, J.A., Parikh, N.D., Murphy, C., McCallister, K., Singal, A.G., 2017. An assessment of benefits and harms of hepatocellular carcinoma surveillance in patients with cirrhosis. Hepatology 65, 1196–1205. https://doi.org/10.1002/hep.28895.

Bialecki, E.S., Di Bisceglie, A.M., 2005. Diagnosis of hepatocellular carcinoma. HPB 7, 26–34. https://doi.org/10.1080/13651820410024049.

Chaudhary, C., Kumar, S., Chandra, R., 2021. Hierarchical structure of molybdenum disulfide-reduced graphene oxide nanocomposite for the development of a highly efficient serotonin biosensing platform. New J. Chem. 45, 18623–18634. https://doi.org/10.1039/d1nj03534g.

Chauhan, D., Chandra, R., Kumar, S., 2021. Advanced electrochemical nanobiosensor for ultraefficient Annexin A2 biomarker detection: a rapid, label free and minimal invasive approach towards early diagnosis of liver cancer. Mater. Lett. 305, 130856 https://doi.org/10.1016/j.matlet.2021.130856.

Chen, S., Yuan, B., Liu, G., Zhang, D., 2020. Electrochemical sensors based on covalent organic frameworks: a critical review. Front. Chem. 8, 1–11. https://doi.org/10.3389/fchem.2020.601044.

Chen, X., Gao, P., Guo, L., Zhang, S., 2015. Graphdiyne as a promising material for detecting amino acids. Sci. Rep. 5, 1–9. https://doi.org/10.1038/srep16720.

Das, N., Basu, J., RoyChaudhuri, C., 2015. Graphene coated nanoporous silicon immunosensor for food toxin detection. Int. J. Adv. Eng. Sci. Appl. Math. 7, 204–209. https://doi.org/10.1007/s12572-015-0144-z.

Dasgupta, P., Henshaw, C., Youlden, D.R., Clark, P.J., Aitken, J.F., Baade, P.D., 2020. Global trends in incidence rates of primary adult liver cancers: a systematic review and meta-analysis. Front. Oncol. 10, 1–17. https://doi.org/10.3389/fonc.2020.00171.

Ding, C., Zhao, F., Ren, R., Lin, J.M., 2009. An electrochemical biosensor for α-fetoprotein based on carbon paste electrode constructed of room temperature ionic liquid and gold nanoparticles. Talanta 78, 1148–1154. https://doi.org/10.1016/j.talanta.2009.01.036.

El-Abd, N., Fawzy, A., Elbaz, T., Hamdy, S., 2016. Evaluation of annexin A2 and as potential biomarkers for hepatocellular carcinoma. Tumor Biol. 37, 211–216. https://doi.org/10.1007/s13277-015-3524-x.

Gong, Y., Shen, L., Kang, Z., Liu, K., Du, Q., Ye, D., Zhao, H., Sun, X.A., Zhang, J., 2020. Progress in energy-related graphyne-based materials: advanced synthesis, functional mechanisms and applications. J. Mater. Chem. 8, 21408–21433. https://doi.org/10.1039/d0ta08521a.

He, J., Wang, N., Cui, Z., Du, H., Fu, L., Huang, C., Yang, Z., Shen, X., Yi, Y., Tu, Z., Li, Y., 2017. Hydrogen substituted graphdiyne as carbon-rich flexible electrode for lithium and sodium ion batteries. Nat. Commun. 8, 1–11. https://doi.org/10.1038/s41467-017-01202-2.

Holder, C.F., Schaak, R.E., 2019. Tutorial on powder X-ray diffraction for characterizing nanoscale materials. ACS Nano 13, 7359–7365. https://doi.org/10.1021/acsnano.9b05157.

Huang, C., Li, Yongjun, Wang, N., Xue, Y., Zuo, Z., Liu, H., Li, Yuliang, 2018. Progress in research into 2D graphdiyne-based materials. Chem. Rev. 118, 7744–7803. https://doi.org/10.1021/acs.chemrev.8b00288.

Hui, N., Sun, X., Song, Z., Niu, S., Luo, X., 2016. Gold nanoparticles and polyethylene glycols functionalized conducting polyaniline nanowires for ultrasensitive and low fouling immunosensing of alpha-fetoprotein. Biosens. Bioelectron. 86, 143–149. https://doi.org/10.1016/j.bios.2016.06.028.

Jain, R., Nirbhaya, V., Chandra, R., Kumar, S., 2021. Nanostructured mesoporous carbon based electrochemical biosensor for efficient detection of swine flu. Electroanalysis 34, 43–55.

Kumar, S., Gupta, N., Malhotra, B.D., 2021b. Ultrasensitive biosensing platform based on yttria doped zirconia-reduced graphene oxide nanocomposite for detection of salivary oral cancer biomarker. Bioelectrochemistry 140, 107799. https://doi.org/10.1016/j.bioelechem.2021.107799.

Kumar, R., Naz Ansari, S., Deka, R., Kumar, P., Saraf, M., Mobin, S.M., 2021a. Progress and perspectives on covalent-organic frameworks (COFs) and composites for various energy applications. Chem. Eur J. 27, 13669–13698. https://doi.org/10.1002/chem.202101587.

Kumar, S., Panwar, S., Kumar, Saurabh, Augustine, S., Malhotra, B.D., 2019. Biofunctionalized nanostructured yttria modified non-invasive impedometric biosensor for efficient detection of oral cancer. Nanomaterials 9. https://doi.org/10.3390/nano9091190.

Li, J., Wan, C., Wang, C., Zhang, H., Chen, X., 2020. 2D material Chemistry: graphdiyne-based biochemical sensing. Chem. Res. Chin. Univ. 36, 622–630. https://doi.org/10.1007/s40242-020-0181-4.

Madureira, P.A., Waisman, D.M., 2013. Annexin A2: the importance of being redox sensitive. Int. J. Mol. Sci. 14, 3568–3594. https://doi.org/10.3390/ijms14023568.

Marrero, J.A., Kulik, L.M., Sirlin, C.B., Zhu, A.X., Finn, R.S., Abecassis, M.M., Roberts, L. R., Heimbach, J.K., 2018. Diagnosis, staging, and management of hepatocellular carcinoma: 2018 practice guidance by the American association for the study of liver diseases. Hepatology 68, 723–750. https://doi.org/10.1002/hep.29913.

Parvin, N., Jin, Q., Wei, Y., Yu, R., Zheng, B., Huang, L., Zhang, Y., Wang, L., Zhang, H., Gao, M., Zhao, H., Hu, W., Li, Y., Wang, D., 2017. Few-layer graphdiyne nanosheets applied for multiplexed real-time DNA detection. Adv. Mater. 29, 1–7. https://doi.org/10.1002/adma.201606755.

Pavia, D.L., Lampman, G.M., Kriz, G.S., Vyvyan, J.R., 2010. Introduction to Spectroscopy, Fourth. Cengage Learning.

Sun, Y., Gao, G., Cai, J., Wang, Y., Qu, X., He, L., Liu, F., Zhang, Y., Lin, K., Ma, S., Yang, X., Qian, X., Zhao, X., 2013. Annexin A2 is a discriminative serological candidate in early hepatocellular carcinoma. Carcinogenesis 34, 595–604. https://doi.org/10.1093/carcin/bgs372.

Vannozzi, L., Catalano, E., Telkhozhayeva, M., Teblum, E., Yarmolenko, A., Avraham, E. S., Konar, R., Nessim, G.D., Ricotti, L., 2021. Graphene oxide and reduced graphene oxide nanoflakes coated with glycol chitosan, propylene glycol alginate, and polydopamine: characterization and cytotoxicity in human chondrocytes. Nanomaterials 11. https://doi.org/10.3390/nano11082105.

Wang, N., He, J., Wang, K., Zhao, Y., Jiu, T., Huang, C., Li, Y., 2019. Graphdiyne-based materials: preparation and application for electrochemical energy storage. Adv. Mater. 31, 1–22. https://doi.org/10.1002/adma.201803202.

[WWW Document] WHO Fact sheet, 2021, URL, accessed 11.10.21. https://www.who.int/news-room/fact-sheets/detail/cancer.

Wu, M.X., Yang, Y.W., 2017. Applications of covalent organic frameworks (COFs): from gas storage and separation to drug delivery. Chin. Chem. Lett. 28, 1135–1143. https://doi.org/10.1016/j.cclet.2017.03.026.

Zhang, M., Wang, X., Sun, H., Wang, Naiyin, He, J., Wang, Ning, Long, Y., Huang, C., Huang, C., Li, Y., 2020. Induced ferromagnetic order of graphdiyne semiconductors by introducing a heteroatom. ACS Cent. Sci. 6, 950–958. https://doi.org/10.1021/acscentsci.0c00348.

Zhang, Y., Huang, X., Luo, F., Lei, Y., Chen, L., Weng, Z., Guo, L., Lin, Z., 2018. Highly sensitive electrochemical immunosensor for golgi protein 73 based on proximity ligation assay and enzyme-powered recycling amplification. Anal. Chim. Acta 1040, 150–157. https://doi.org/10.1016/j.aca.2018.08.021.

Zhao, Y., Zhang, L., Qi, J., Jin, Q., Lin, K., Wang, D., 2018. Graphdiyne with enhanced ability for electron transfer. Acta Physico-chimica Sin. 34, 1048–1060. https://doi.org/10.3866/PKU.WHXB201802281.